PHILOSOPHICAL TRANSACTIONS OF THE ROYAL SOCIETY A MATHEMATICAL, PHYSICAL & ENGINEERING SCIENCES

Metal–insulator transitions and giant magnetoresistance in perovskite oxides

C. N. R. Rao

Phil. Trans. R. Soc. Lond. A 1998 **356**, 23-39
doi: 10.1098/rsta.1998.0147

The Royal Society

Metal–insulator transitions and giant magnetoresistance in perovskite oxides

By C. N. R. Rao

Solid State and Structural Chemistry Unit and CSIR Centre of Excellence in Chemistry, Indian Institute of Science, Bangalore 560012, India
Materials Research Laboratory, University of California, Santa Barbara, CA 93106-5050, USA

Transition-metal oxides of perovskite structure exhibit compositionally controlled metal–insulator (M–I) transitions wherein the temperature coefficient of resistivity changes sign at a resistivity value close to Mott's maximum metallic resistivity. These oxides also obey the Mott criterion, $n_c^{1/3} a_H \approx 0.25$, arising from electron interactions. Cuprate superconductors, in spite of their anomalous properties in the metallic state, obey the above two criteria for metallicity. The cuprates also exhibit unusual insulator–superconductor and M–I transitions. Perovskite manganates which exhibit giant magnetoresistance, on the other hand, show high resistivities ($\rho > \rho_{max}$ of Mott) at low temperatures, in the 'metallic' state, and the mechanism of the M–I transition in these materials is not clear. Jahn–Teller distortion and charge ordering compete with double exchange and the electronic properties are accordingly determined by the dominant interaction. While double exchange favours ferromagnetism and metallicity, charge-ordering and Jahn–Teller effects favour insulating behaviour. Charge ordering in the manganates is specially interesting being strongly affected by the size of the A-site cations.

Keywords: perovskite oxides; cuprate superconductors; giant magnetoresistance; rare earth manganates; charge ordering; spin ordering

1. Introduction

Of all the classes of materials, transition-metal oxides probably exhibit the widest range of electrical resistivity (10^{-10}–$10^{20}\ \Omega$ cm). Besides the oxides with metallic behaviour (e.g. ReO_3, RuO_2), there are oxides which undergo transitions from insulating to the metallic state, V_2O_3 being the most well-known example with a 10 million fold jump in resistivity at 150 K due to the metal–insulator transition (Rao 1989). Of all the metal-oxide systems, those with the perovskite structure with the general composition ABO_3 are particularly fascinating because of their unique structural features (Rao & Raveau 1995). Thus, in the ideal cubic structure, 180° cation–anion–cation (cac) interaction is possible. The cac angle deviates from 180° when the structure distorts from cubic symmetry to lower ones. The relative sizes of the cations in the A and B sites determine the extent of distortion and hence the cac angle. Perovskite oxides such as $LaNiO_3$ and $SrRuO_3$ are metallic. There are several perovskite systems which exhibit compositionally controlled metal–insulator (M–I) transitions (Rao & Ganguly 1985). $LaCoO_3$ which is an insulator at ordinary temperatures, becomes metallic when La is progressively substituted by Sr. $La_{1-x}Sr_xCoO_3$

($x \geqslant 0.3$) is a ferromagnetic metal. A different type of example would be that of $LaNi_{1-x}Mn_xO_3$ which becomes insulating as x increases. We shall briefly examine such perovskite oxides exhibiting M–I transitions across a state which can be considered to be marginally metallic. All these oxides, however, conform to the known criteria of metallicity (Rao 1996). The cuprates which exhibit high-temperature superconductivity also possess the perovskite motif (Rao & Ganguli 1995) and are marginally metallic in the normal state, with certain anomalous properties. Yet, they obey some of the traditional criteria for metallicity. We shall briefly discuss M–I and related transitions of cuprates.

Perovskite manganates of the general formula $Ln_{1-x}A_xMnO_3$ (where Ln denotes rare earths and A denotes alkaline earths) have created wide interest recently because they exhibit giant magnetoresistance (Rao *et al.* 1996). These oxides become ferromagnetic at an optimal value of x (or Mn^{4+} content) and undergo an insulator–metal transition around the ferromagnetic Tc. These properties are attributed to double exchange (Zener 1951) associated with electron hopping from Mn^{3+} to Mn^{4+}. The double exchange which favours itinerant electron behaviour is opposed by the Jahn–Teller distortion due to the presence of Mn^{3+}. These manganates exhibit rather unusually high resistivities even in the so-called metallic regime and do not obey the criteria for metallicity. Furthermore, the manganates show charge-ordering specially when the size of the A-site cations is small. Charge ordering competes with double exchange and favours insulating behaviour. Thus, the manganates exhibit a variety of properties associated with spin, charge as well as orbital ordering. We shall discuss some important aspects of giant magnetoresistance, charge ordering and related properties of the manganates in some detail.

2. Metal–insulator transitions in perovskite oxides

Two typical compositionally controlled M–I transitions in perovskite oxide systems are shown in figure 1. In $La_{1-x}Sr_xCoO_3$, the material becomes metallic as x is increased beyond a critical composition; a similar behaviour is seen in $La_{1-x}Sr_xVO_3$ (Rao & Ganguly 1985). Metallicity arises in these oxides because of the fast hopping of electrons between the 3+ and 4+ states of the transition metal. It is interesting that the temperature coefficient of resistivity changes sign around a resistivity value close to Mott's maximum resistivity, ρ_{max} (Mott 1972). In $LaNi_{1-x}Mn_xO_3$ where the material becomes insulating with increasing x, the change from the metallic to the insulating state occurs again around Mott's ρ_{max}. The value of ρ_{max} or σ_{min} is known to scale with the critical carrier concentration, n_c (Mott 1982). In figure 2, $\log \rho_{max}$ is plotted against $\log n_c$ for a variety of systems including doped semiconductors. The points corresponding to the metal oxides exhibiting compositionally controlled metal–insulator transitions fall in line with the other electronic materials at the threshold of metallicity. These oxides not only obey the ρ_{max} or the σ_{min} criterion arising from considerations of disorder, but also the $n_c^{1/3}a_H \approx 0.25$ criterion arising from electron interactions (Mott 1961). Although the oxides obey the σ_{min} criterion, it is possible that some of them may show a departure from this behaviour and become insulating at very low temperatures (around 50 K or below), with the resistivity increasing with decrease in temperature as shown by Raychaudhuri (1991) (i.e. conductivity is not zero at 0 K). It appears that σ_{min} or ρ_{max} serves as the high-temperature limit for the conductivity of these marginally metallic oxides. Certainly, ρ_{max} signifies the value of resistivity where the temperature coefficient changes sign.

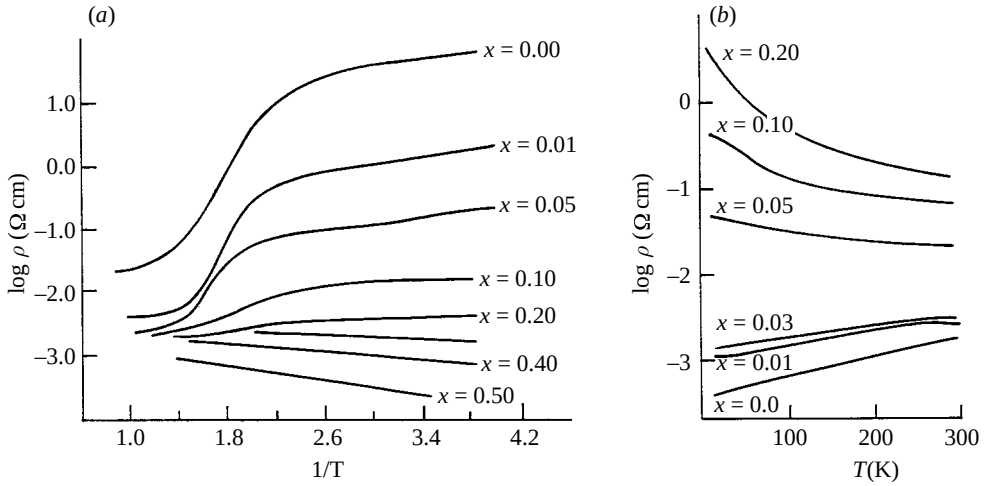

Figure 1. Compositionally controlled metal–insulator transitions in (*a*) $La_{1-x}Sr_xCoO_3$ and (*b*) $LaNi_{1-x}Mn_xO_3$ (from Rao & Ganguly 1985).

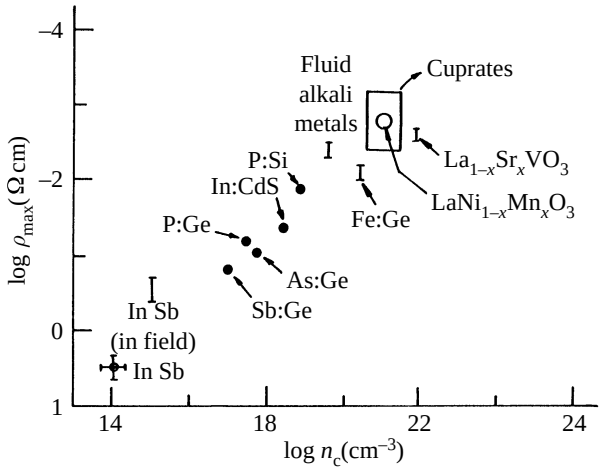

Figure 2. A log–log plot of Mott's maximum metallic resistivity, ρ_{max}, against the critical carrier density, n_c, at the metal–insulator transition.

Photoelectron spectroscopic studies of $La_{1-x}Sr_xCoO_3$ and $LaNi_{1-x}Mn_xO_3$ in the valence band region have shown the presence of a finite density of states at the Fermi level in the oxides (Edwards & Rao 1995).

3. Cuprate superconductors

The cuprates which exhibit high-temperature superconductivity generally exhibit metallic type resistivity (with the resistivity decreasing with temperature) before they become superconducting. The values of resistivities in the metallic regime before they become superconducting in many of them is in the 2–5 mΩ cm range, not far from Mott's ρ_{max}. The cuprates obey the $n_c^{1/3}a_H \approx 0.25$ relation as shown in figure 3, besides following the linear $\log \sigma_{min}$–$\log n_c$ plot (figure 2). Although these observations suggest that the cuprates are similar to $La_{1-x}Sr_xVO_3$ and other oxides showing

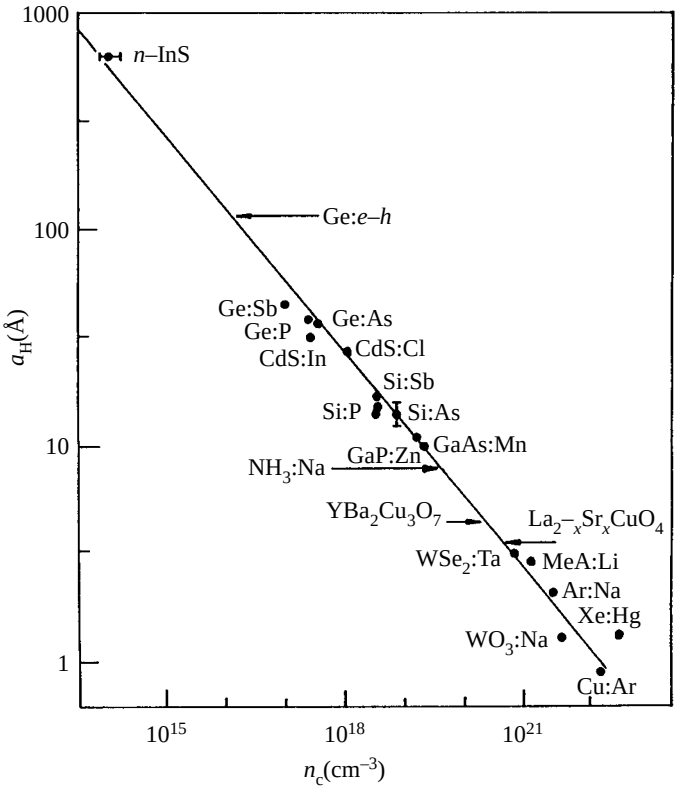

Figure 3. Relation between the critical carrier concentration, n_c, and the Bohr radius, a_H. The solid line represents $n_c^{1/3} a_H = 0.26$ (from Thomas (1983) and Edwards & Sienko (1978)).

M–I transitions, they exhibit many anomalous properties in the metallic state, one of them being the linear variation of resistivity with temperature in the metallic state. The cuprates reveal the presence of strong correlation effects and there is as yet no unanimous view as to the best way of describing the marginally metallic state. High-energy spectroscopic studies of the cuprates show the oxygen 2p contribution to the hole-doped states near the Fermi level to be significant.

The cuprates exhibit compositionally controlled metal–insulator transitions in the normal state ($T > T_c$) as can be seen in figure 4*a*, *b*. It is rather unusual that the insulating state directly transforms to the superconducting state in some of the cuprates (figure 4*b*). Such an insulator–metal transition is found in $La_{2-x}Sr_xCuO_4$ as well. It is interesting to ponder whether there can be insulating and superconducting ground states without a metallic ground state in between. A careful comparison has shown that the Hall coefficients and other properties of such cuprate compositions are different from those of oxide systems such as $La_{1-x}Sr_xTiO_3$ which exhibit insulator–metal transitions (Iye 1995).

4. Giant magnetoresistance and metal–insulator transitions in rare earth manganates

$LaMnO_3$ is an insulator with an orthorhombically distorted perovskite structure ($b > a > c^{1/2}$, *Pbnm*) and typically contains some Mn^{4+} as prepared by the usual

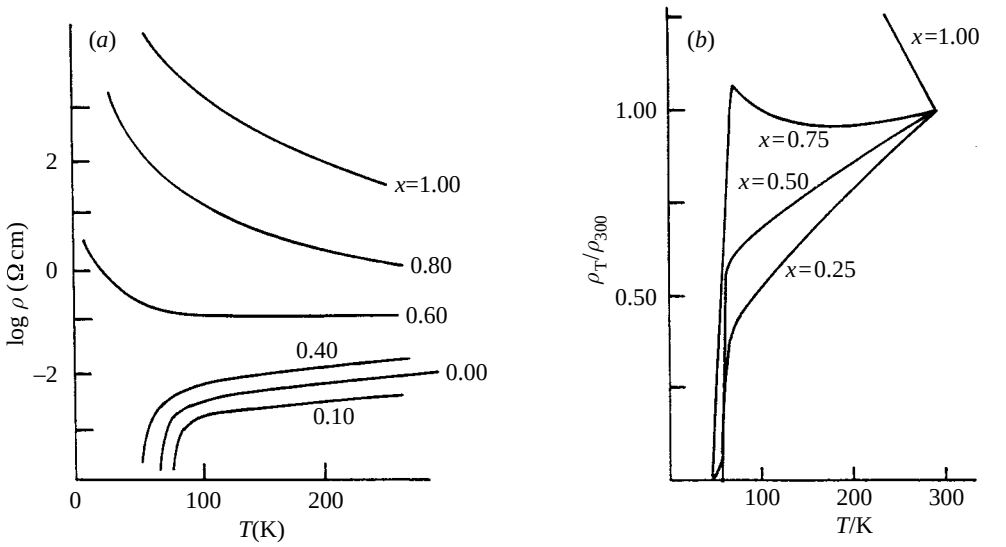

Figure 4. Temperature variation of resistivity in superconducting cuprates: (*a*) $Bi_2Ca_{1-x}Y_xSr_2Cu_2O_8$, (*b*) $TlCa_{1-x}Nd_xSr_2CuO_6$ (from the author's laboratory).

solid state reactions. $LaMnO_3$ with a small proportion of Mn^{4+} ($\lesssim 5\%$) becomes antiferromagnetically ordered at low temperatures ($T_N \sim 150$ K). When the La^{3+} in $LaMnO_3$ is progressively substituted by a divalent cation as in $La_{1-x}A_xMnO_3$ (A = Ca, Sr or Ba), it becomes ferromagnetic with a well-defined Curie temperature, T_c, and metallic below T_c (Jonker & van Santen 1950; Rao *et al.* 1996). The saturation moment is typically approximately $3.8\mu_B$ which is close to the theoretical estimate based on localized spin-only moments, suggesting that the carriers are spin polarized. Below T_c, the manganates exhibit metal-like conductivity. Figure 5 illustrates how the ferromagnetism and the M–I transition occur around T_c in a typical $La_{1-x}Ca_xMnO_3$ composition (Mahendiran *et al.* 1996*a*). The simultaneous observation of itinerant electron behaviour and ferromagnetism in the manganates is explained by Zener's double-exchange mechanism. The basic process in this mechanism is the hopping of a d-hole from Mn^{4+} (d^3, t_{2g}^3, $S = \frac{3}{2}$) to Mn^{3+} (d^3, $t_{2g}^3e_g^1$, $S = 2$) via the oxygen, so that the Mn^{4+} and Mn^{3+} ions change places. The t_{2g}^3 electrons of the Mn^{3+} ion are localized on the Mn site giving rise to a local spin of $\frac{3}{2}$, but the e_g state, which is hybridized with the oxygen 2p state, can be localized or itinerant. There is strong Hund's rule interaction between the e_g and the t_{2g}^3 electrons. Goodenough (1971) has pointed out that the ferromagnetism is governed not only by double exchange, but also by the nature of the super-exchange interactions. It may be noted that the Mn^{3+}–O–Mn^{4+} superexchange interaction is ferromagnetic while both the Mn^{3+}–O–Mn^{3+} and Mn^{4+}–O–Mn^{4+} interactions are antiferromagnetic.

The orthorhombic distortion of $LaMnO_3$ decreases as La is progressively substituted by a divalent ion and until it becomes rhombohedral or pseudo-cubic. The Mn–O–Mn angle approaches 180° as the distortion decreases. When the size of the A-site cations becomes small, orthorhombic distortion is favoured. The key factor responsible for the distortion in $LaMnO_3$ is the Jahn–Teller distortion due to Mn^{3+} ions ($t_{2g}^3e_g^1$). Accordingly, $LaMnO_3$ has three Mn–O distances (1.91, 1.96 and 2.19 Å). Across the M–I transition, the Jahn–Teller distortion increases in $Ln_{1-x}A_xMnO_3$, the distortion being greater in the insulating regime (Garcia-Munoz *et al.* 1997).

Increasing static coherent MnO_6 distortion is associated with increasing insulating behaviour and decreasing T_c (Radaelli *et al.* 1996). The structural parameters, specifically the oxygen thermal parameters, show a significant change across the M–I transition. Clearly, Mn^{4+} ions decrease the Jahn–Teller distortion, increase the itinerancy of electrons through double exchange and increase the tolerance factor of the pervoskite structure (since Mn^{4+} is smaller than Mn^{3+}). Temperature-composition phase diagrams for $La_{1-x}A_xMnO_3$ have been worked out with increasing x or Mn^{4+} content (Rao *et al.* 1996). A composition of $x \sim 0.3$ is ideal to observe a good M–I transition and negative giant magnetoresistance (GMR). The magnitude of GMR is maximum at the M–I transition (figure 5) and scales with the field-induced magnetization (Urushibara *et al.* 1995).

GMR is found over a wide range of compositions of $La_{1-x}Ca_xMnO_3$ ($x < 0.5$). However, this material shows significant lattice effects in particular for low x. When $x = 0.2$, a local structural distortion occurs due to the formation of lattice polarons which arises from the strong electron–lattice coupling (Brillinge *et al.* 1996). EXAFS studies reveal significant changes in the local structure in the $x = 0.3$ composition in the 80–300 K range which are attributed to the formation of small polarons due to the Jahn–Teller distortion when $T > T_c$ (Tyson *et al.* 1996). Lattice polaron formation and local structural distortion have important implications on the electron transport (high resistivity) in these materials. $La_{1-x}Sr_xMnO_3$ is somewhat different from $La_{1-x}Ca_xMnO_3$, the A-site ion size being larger. The ferromagnetic metallic regime in $La_{1-x}Sr_xMnO_3$ extends over larger values of x and the Curie temperatures are higher. Electron transport and magnetic properties of the $x = 0.3$ compositions of the Ca and Sr compositions have been investigated in thin films as well as in bulk materials (Snyder *et al.* 1996). While the magnetization decreases as T^2, the resistivity increases proportional to T^2. A study of $La_{0.7}Sr_{0.3}MnO_3$ by neutron scattering has shown that the spin dynamics and the magnetic critical scattering are surprisingly comparable to those of typical metallic ferromagnets (Martin *et al.* 1996). In $La_{1-x}Sr_xMnO_3$ ($x = 0.17$), the local spin moments and charge carriers couple strongly to changes in the structure and the structure can be switched by the application of a magnetic field depending on the temperature. The magnetic field which causes this cross-over from the orthorhombic to the rhombohedral structure is rather low (around $2T$), showing thereby that a very small energy difference exists between these two structures (Asamitsu *et al.* 1996*a*). When $x = 0.1$ and 0.15, a polaron-ordered phase is formed and the polaron lattice has a tendency to lock into a commensurate structure when $x = 0.125$ (Yamada *et al.* 1996). Evidence for magnetic polarons at $T > T_c$ has been found in $(LaY)_{0.67}Ca_{0.33}MnO_3$, with 12 Å localized magnetic clusters which grow under magnetic fields (De Teresa *et al.* 1997).

Hydrostatic pressure stabilizes the ferromagnetic metallic state in $La_{1-x}A_xMnO_3$ (i.e. increases the T_c). Hydrostatic pressure enhances the Mn–O–Mn transfer integral through a change in the Mn–O–Mn angle. A similar effect can be brought about by increasing the radius of the A-site cation. There is a direct relationship between T_c and the average radius of the A-site cation, $\langle r_A \rangle$, the T_c increasing with $\langle r_A \rangle$ (Hwang *et al.* 1995; Fontcuberta *et al.* 1996). A small $\langle r_A \rangle$ gives rise to a distortion of the MnO_6 octahedra by bending the Mn–O–Mn bond and in turn causing the narrowing of the e_g bandwidth to a greater extent. Accordingly, yttrium substitution in $La_{1-x}A_xMnO_3$ decreases T_c, and enhances the magnitudes of resistivity as well as magnetoresistance (Ibarra *et al.* 1995; Mahendiran *et al.* 1996*b*). By plotting the T_c against $\langle r_A \rangle$, one obtains a phase diagram separating the ferromagnetic metal and

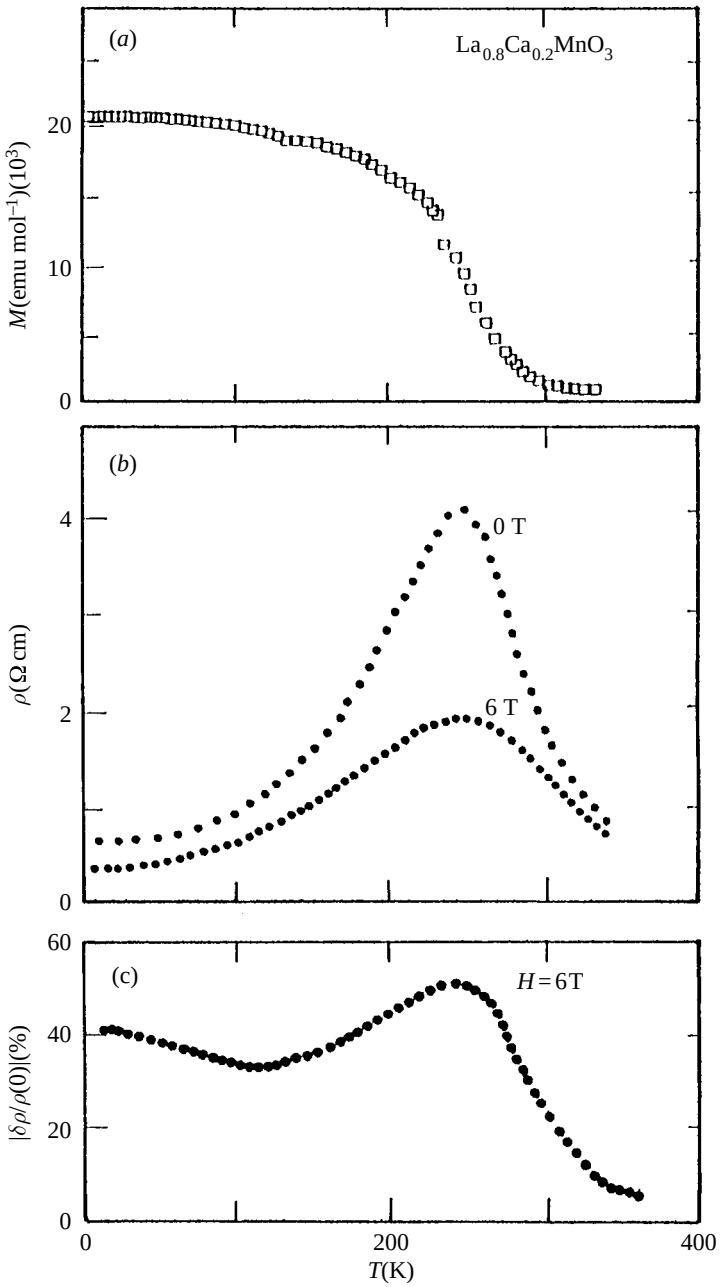

Figure 5. Temperature variation of (*a*) magnetization, (*b*) resistivity (at $H = 0$ T and 6 T) and (*c*) magnetoresistance in $La_{0.8}Ca_{0.2}MnO_3$ (from Mahendiran *et al.* 1996*a*).

paramagnetic insulator regimes (Hwang *et al.* 1995; Mahesh *et al.* 1995). In figure 6, we show a phase diagram obtained in this manner. In the left-hand bottom corner, we see the ferromagnetic insulator regime. GMR generally decreases with increase in $\langle r_A \rangle$, just as the peak resistivity at the M–I transition. Enhanced GMR could arise from a reduced mobility of the doping holes and an increase in the coupling between the localized and itinerant electrons (Fontecuberta *et al.* 1996). The enhanced GMR

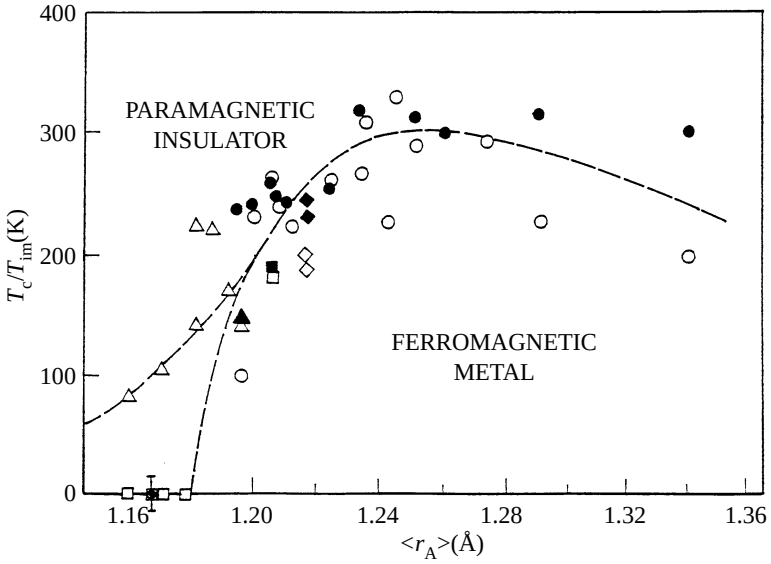

Figure 6. Variation of ferromagnetic T_c or M–I transition temperature T_{im} in $Ln_{1-x}A_xMnO_3$ with the weighted average radius of the A-site cations, $\langle r_A \rangle$ (from Mahesh *et al.* 1995).

in materials with low T_c (and hence small bandwidth) could also arise as an effect of the magnetic field on the electron–lattice interaction.

The effect of particle size on the electron transport and magnetic properties of polycrystalline $La_{0.7}Ca_{0.3}MnO_3$ has been investigated (Mahesh *et al.* 1996*a*). Although T_c decreases with the decreasing particle size, the magnetoresistance is insensitive to particle size. The M–I transition becomes broader when the particle size is small, but the percentage MR is nearly constant over a wide temperature range. The low-temperature MR is significantly dependent on the grain size. For larger grain size, the MR at the lowest temperature decreases eventually becoming zero as in good single crystals. Samples of manganates with different particle sizes prepared with different heat treatments often show large differences between the ferromagnetic T_c and the temperature of the M–I transition (Mahendiran *et al.* 1996*c*). Clearly, grain boundaries contribute substantially to magnetoresistance in polycrystalline materials, in particular at $T \ll T_c$.

The effect of dimensionality on GMR and related properties have been studied by examining the $(SrO)(La_{1-x}Sr_xMnO_3)_n$ family (Mahesh *et al.* 1996*b*; Moritomo *et al.* 1996). The $n = 1$ member which is two dimensional with the K_2NiF_4 structure is an insulator, while the $n = \infty$ member is the three-dimensional perovskite showing GMR and other properties. The $n = 2$ member exhibits the sharpest I–M transition and high MR. A recent study of $La_{1.4}Sr_{1.6}Mn_2O_7$ (Kimura *et al.* 1996) has shown that the current perpendicular to the MnO_2 planes is large, particularly close to T_c and the barrier to transport provided by the intervening insulating layers is removed by the magnetic field. Interlayer transport seems to involve tunnelling.

5. Unusual features of rare earth manganates

Studies of the electrical, magnetic and other properties of $Ln_{1-x}A_xMnO_3$ systems have revealed certain unusual features with respect to the charge carriers in

these oxides. The manganates exhibit high resistivities even in the metallic state, particularly at low temperatures (Coey *et al.* 1995). The values of resistivities are considerably higher than Mott's value of maximum metallic resistivity in many of these materials (Mahendiran *et al.* 1996*a*), the resistivity reaching constant values as high as 10^3–$10^4\ \Omega$ cm at low temperatures. A clear picture of the nature of carriers responsible for the high resistivity is yet to emerge. The cause of the observed temperature dependence of resistivity at low temperatures is also not entirely clear. Another unusual feature of the manganates is related to the occurrence of large MR in a small field at relatively high temperatures. The scale of Zeeman energy associated with a field of 1 T in these spin systems is approximately 5 K. This is much too small compared to the scale of thermal energy (200–300 K) where one sees such a large MR.

Optical conductivity measurements on $La_{0.825}Sr_{0.125}MnO_3$ in the range 0–10 eV show a band of 1.5 eV and the spectral weight is transferred from this band with decreasing temperature. The 1.5 eV band is due to interband transitions between the exchange split spin polarized e_g bands. At $T < T_c$, intraband transitions in the e_g band dominate the spectrum (Okimoto *et al.* 1995). Photoemission studies of $La_{1-x}Sr_xMnO_3$ show the density of states near the Fermi level even in the metallic state to be negligible (Sarma *et al.* 1996). The density of states rises rapidly with energy very close to E_F. There is a transfer of spectral weight from the unoccupied states to occupied states with decrease in hole doping. The redistribution of spectral weight in the photoemission spectra is attributed to a change in the electron correlation strength induced by the changing degree of ferromagnetic order with temperature. The density of states at the Fermi level is much lower in the insulator regime than in the metallic regime of the manganates (Park *et al.* 1996). Mn 2p resonant photoemission and O 1s X-ray absorption studies have shown that the band gap collapses around T_c with an increase in the density of states near the Fermi level on cooling. In the insulating state above T_c, small polaron effects seem to present. A recent study of tunnelling density of states by low temperature STM in $La_{0.8}Ca_{0.2}MnO_3$ has, however, shown that at $T < T_c$, a large number of states become available near E_F (Biswas & Raychaudhuri 1996). The specific heat of the metallic samples $La_{0.7}Ba_{0.3}MnO_3$ and $La_{0.8}Ca_{0.2}MnO_3$ give a value of γ (for the linear term) in the region of 4–6 mJ mole^{-1} K^{-2} (Hamilton *et al.* 1996). From the cubic term, the Debye temperature is approximately 400 K. The γ term is significantly enhanced from the free electron and the band values, the enhancement arising from correlation effects and electron–lattice interaction. This γ value is comparable to that in a number of similar metallic ABO_3 perovskites and is not unusual and does not show any indication of depletion of the density of states at the Fermi level.

The Hall coefficient has been measured in epitaxial films of $La_{0.67}Ca_{0.33}MnO_3$ and $La_{0.67}Sr_{0.33}MnO_3$ grown by MOCVD (Snyder *et al.* 1996) and the carrier concentration estimated from the Hall effect is more than that calculated with the assumption that each Mn^{4+} contributes one hole and that all the holes are mobile. For the Sr-doped sample, it is 2.1 holes per Mn and for Ca-doped samples it is 0.9 holes per Mn. This observation is not compatible with the low density of states found from photoemission experiments. While both the specific heat and Hall measurements are sensitive to the bulk, the photoemission measurements are sensitive to the surface. It is not clear if this difference arises from significant differences between the bulk and the surface. In particular, how the density of states and the carrier concentration change as the sample is cooled through T_c need to be examined.

The Seebeck coefficient in several rare earth manganates show a positive peak in the composition range and at a temperature where MR also peaks and becomes more negative with the increase in Mn^{4+} content (Mahendiran *et al.* 1996*a*, *d*). The Seebeck coefficient of $La_{1-x}Sr_xMnO_3$ shows a change in sign from positive to negative at the M–I transition boundary or at $T < T_c$ depending on the composition (Asamitsu *et al.* 1996*b*). An anomalous change in the electronic structure with spin-polarization may occur when $x = 0.2$–0.3. Based on the pressure dependence of the Seebeck coefficient, it has been suggested that there is a crossover from a polaronic to extended state electronic conduction at T_c (Archibald *et al.* 1996).

Double exchange seems necessary for the GMR of the manganate system as recently shown by a study of the $LnMn_{1-x}Cr_xO_3$ system where Cr^{3+} replaces Mn^{4+} (Gundakaram *et al.* 1996). The basic question that remains is why these manganates are insulating when $T > T_c$. The anomalous resistance has been explained by Millis *et al.* (1996) by considering electron–phonon interaction arising from the Jahn–Teller splitting of the Mn d levels. Jahn–Teller distortion localizes conduction electrons as polarons. As the temperature decreases, the transfer integral, t_{ij}, increases and the ratio of the Jahn–Teller energy to t_{ij} decreases. The coupling varies with temperature and composition and increases across the metal–insulator transition (Roder *et al.* 1996). The large effect of local lattice distortion and crystal structure symmetry on electron transport and magnetism show that one cannot explain the unusual behaviour without taking the lattice into account. The observed T_c (approximately 250–400 K) in most manganates is considerably lower than that estimated from the measured spin-wave stiffness constant (Lynn *et al.* 1996) implying that the ferromagnetic exchange arising from the double exchange mechanism is not the only factor that effects T_c. The importance of electron–lattice interaction is also indicated by the observation of a large oxygen isotope shift of T_c in $La_{0.8}Ca_{0.2}MnO_3$ (Zhao *et al.* 1996). Besides lattice effects, electron correlation yields a large distribution of spectral weights (Satpathy *et al.* 1996). The electrical resistivity of the rare-earth manganates across the M–I transition is indeed difficult to understand especially at low temperatures based on double-exchange or electron–phonon interaction alone. We also do not understand why GMR actually occurs in these oxides.

6. Charge-ordering and spin-ordering in the manganates

Charge-ordering is not new to transition-metal oxides. Fe_3O_4 undergoes the Verwey transition with a resistivity anomaly due to charge ordering at 120 K and the ferrimagnetic ordering at 860 K. Charge ordering of the Mn^{3+} and Mn^{4+} ions in the perovskite manganates, $Ln_{1-x}A_xMnO_3$ is more interesting and is associated with dramatic changes in properties (Rao *et al.* 1996). Charge ordering in the manganates is strongly dependent on the average radius of the A-site cations, $\langle r_A \rangle$. The ferromagnetic T_c increases with increase in $\langle r_A \rangle$ while charge ordering is favoured by small $\langle r_A \rangle$. Charge ordering and double exchange are thus competing interactions. We shall discuss charge ordering in $Ln_{0.5}A_{0.5}MnO_3$ with equal proportions of Mn^{3+} and Mn^{4+}.

When $\langle r_A \rangle$ is sufficiently large, as in $La_{0.5}Sr_{0.5}MnO_3$ ($\langle r_A \rangle = 1.26$ Å), the manganates become ferromagnetic and undergo an insulator–metal transition around T_c as described earlier. $Nd_{0.5}Sr_{0.5}MnO_3$ with a slightly smaller $\langle r_A \rangle$ (1.236 Å), is ferromagnetic and metallic at 250 K (T_c), but transforms to a charge-ordered (CO) antiferromagnetic state at 150 K (Kuwahara *et al.* 1995). The charge-ordering transition temperature, T_{CO}, is the same as T_N. There is a significant specific heat anomaly

at T_{CO} (T_N) and the resistivity increases markedly due to the metal–insulator (FM–CO) transition as shown in figure 7. This situation is to be contrasted with that of $Nd_{0.5}Ca_{0.5}MnO_3$ ($\langle r_A \rangle = 1.17$ Å) which exhibits a T_{CO} of 250 K in the paramagnetic state (Vogt *et al.* 1996) exhibiting a small heat capacity anomaly. $Nd_{0.5}Ca_{0.5}MnO_3$ is an insulator at all temperatures (figure 7). $Y_{0.5}Ca_{0.5}MnO_3$ with a $\langle r_A \rangle$ of 1.13 Å also gets charge ordered in the paramagnetic state (T_{CO}, 240 K) and becomes antiferromagnetic at 140 K (T_N) (Arulraj *et al.* 1998). In figure 8 we show a simple diagram where we delineate the different types of behaviour of the manganates depending on the $\langle r_A \rangle$. The charge-ordered state of $Nd_{0.5}Sr_{0.5}MnO_3$ is melted by the application of magnetic fields, rendering the material metallic. On the other hand, a magnetic field of 6 T has no effect on the charge-ordered insulating state of $Y_{0.5}Ca_{0.5}MnO_3$ (Arulraj *et al.* 1998). The charge-ordered states in $Nd_{0.5}Sr_{0.5}MnO_3$ and $Nd_{0.5}(Y_{0.5})Ca_{0.5}MnO_3$ are clearly of different kinds, the difference being caused by the difference in $\langle r_A \rangle$. Electronic phase diagrams in the T–H plane can be constructed to show these differences with respect to the M–I transitions effected by magnetic fields, as shown in figure 9 (Tokura *et al.* 1996).

The occurrence of two types of CO states can be understood qualitatively in terms of the variation of the exchange couplings, J_{FM}, J_{AFM} and the single-ion Jahn–Teller energy (E_{JT}) with $\langle r_A \rangle$. While J_{FM} and J_{AFM} are expected to decrease with decrease in $\langle r_A \rangle$, albeit with different slopes, E_{JT} would be insensitive to $\langle r_A \rangle$. In the small-$\langle r_A \rangle$ regime, cooperative Jahn–Teller effect involving long-range elastic strains would dominte charge ordering, while at moderate values of $\langle r_A \rangle$ (when $J_{AFM} > E_{JT}, J_{FM}$), the e_g electrons which are localized magnetically lower the configuration energy by charge ordering. Such a CO state, as exemplified by $Nd_{0.5}Sr_{0.5}MnO_3$, would be sensitive to magnetic fields unlike the manganates such as $Y_{0.5}Ca_{0.5}MnO_3$ in the small-$\langle r_A \rangle$ regime. In $Nd_{0.5}Sr_{0.5}MnO_3$, the gain in Zeeman energy resulting from the application of a magnetic field stabilizes the ferromagnetic metallic state over the antiferromagnetic insulating state. The manganates in the small-$\langle r_A \rangle$ regime can be considered to have pseudo-spins (representing the single ion JT effect) which do not couple to the magnetic field.

A general phase diagram for a fixed composition of the manganates ($Ln_{0.5}A_{0.5}MnO_3$) in the temperature (T)–$\langle r_A \rangle$ plane has been constructed by Kumar & Rao (1997) based on the manner in which J_{FM} and J_{AFM} vary with $\langle r_A \rangle$. The ferromagnetic T_c in the manganates decreases more markedly with $\langle r_A \rangle$ than the T_N values in the manganates, suggesting that J_{FM} decreases more markedly than J_{AFM}. Based on these considerations, a qualitative phase diagram, figure 10, can be drawn. We notice that the highest-temperature phase is always a paramagnetic insulator (PMI) which is paradistortive (PD). The insulating behaviour results from the single-ion Jahn–Teller distortion as well as the blocking of hopping by strong Hund coupling to the paramagnetically disordered Mn spins.

An examination of the different regions of the phase diagram in figure 10 is revealing. In region I, we have the PMI–FMM transition on cooling, as in many of the manganates exhibiting giant magnetoresistance; this region corresponds to region A of figure 8. In region II, $J_{AFM} > J_{FM}$, but the extra entropy of the itinerant carriers in the FM state favours the metallic phase. At low temperatures, however, there would be a first-order FMM–AFMI transition, the latent heat per Mn^{3+} being approximately $k_B T \ln 2$. Region II of figure 10 corresponds to region B of figure 8 and is exemplified by $Nd_{0.5}Sr_{0.5}MnO_3$. In region III, J_{AFM} dominates and a first-order PMI–AFMI transition can occur; at low temperatures, there would be charge

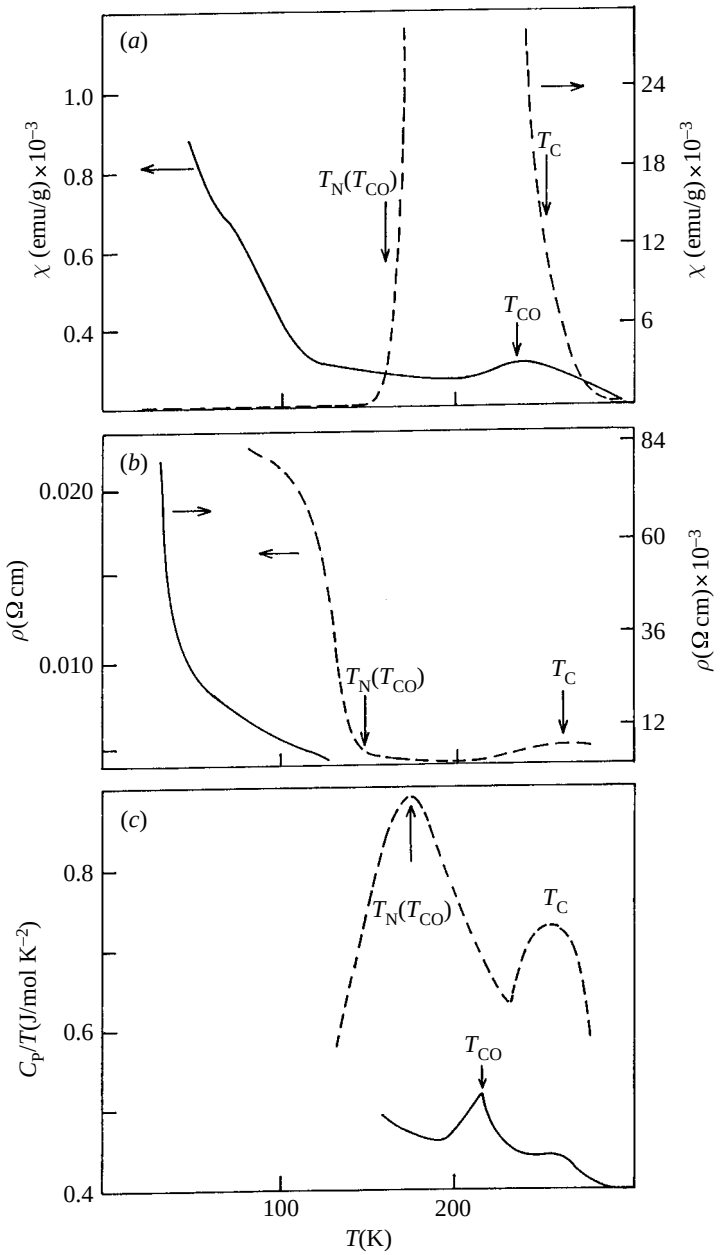

Figure 7. Comparison of the properties of $Nd_{0.5}Sr_{0.5}MnO_3$ ($\langle r_A \rangle = 1.236$ Å) and $N_{0.5}Ca_{0.5}MnO_3$ ($\langle r_A \rangle = 1.17$ Å). Data represented by broken curves correspond to the former.

ordering. Complex magnetic properties can be found in regions III and IV (corresponding to region C in figure 8) arising from the coupling with other parameters (e.g. ferroelastic). Charge ordering in region III is induced by the confinement of carriers by the AFM ordering of the Mn spins, which along with the Hund coupling introduces a spinorial blocking of the Mn^{3+}–O–Mn^{4+} carrier transfer. The associated lattice distortion favours charge-ordering. Region V is dominated by Jahn–Teller

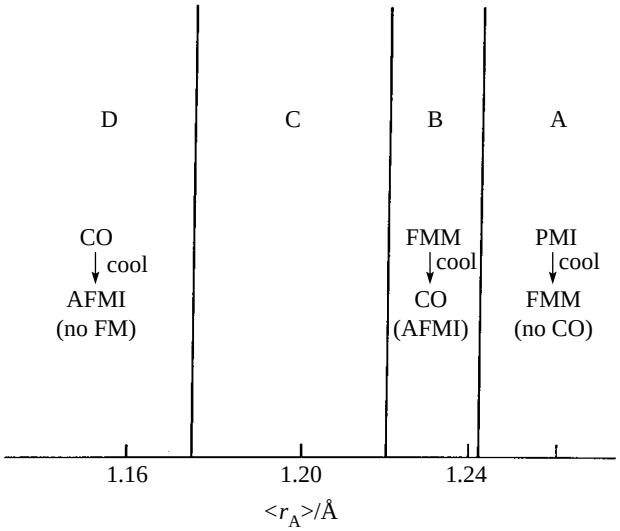

Figure 8. Schematic diagram showing the different types of behaviour of the manganates, $Ln_{0.5}A_{0.5}MnO_3$, depending on $\langle r_A \rangle$. Region A corresponds to the manganates which show ferromagnetism and insulator–metal transitions at T_c while regions B and D correspond to $Nd_{0.5}Sr_{0.5}MnO_3$ and $Y_{0.5}Ca_{0.5}MnO_3$, respectively. Region C would show complex magnetic and related properties. FMM, ferromagnetic metal; PMI, paramagnetic insulator, AFMI, antiferromagnetic insulator, CO, charge-ordered state.

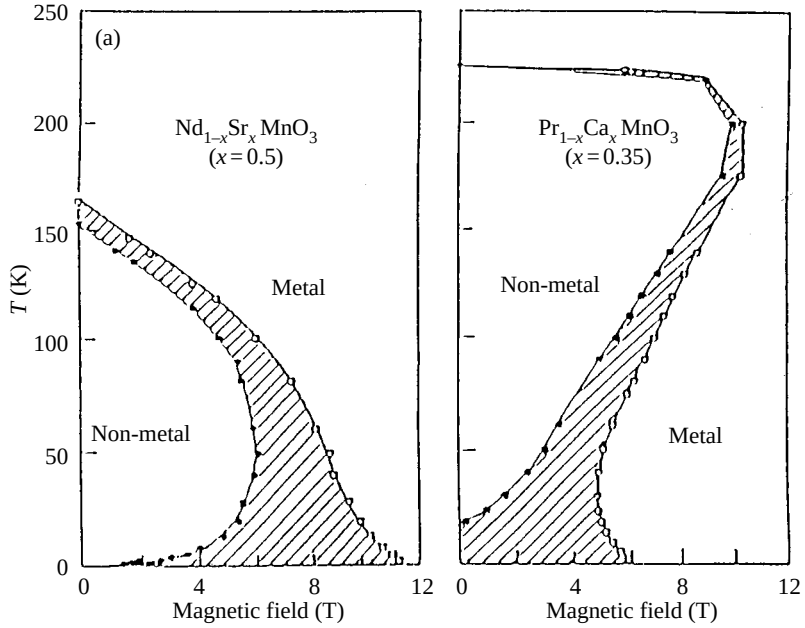

Figure 9. Temperature–magnetic field phase diagram of (*a*) $Nd_{0.5}Sr_{0.5}MnO_3$ and (*b*) $Pr_{0.7}Ca_{0.3}MnO_3$ (from Tokura *et al.* 1996).

effect wherein the pseudo-spin state undergoes a first-order transition (due to loss of communal entropy), on cooling to a FD-insulating phase. Region V corresponds to region D in figure 8 and is exemplified by $Y_{0.5}Ca_{0.5}MnO_3$. Charge-ordering in

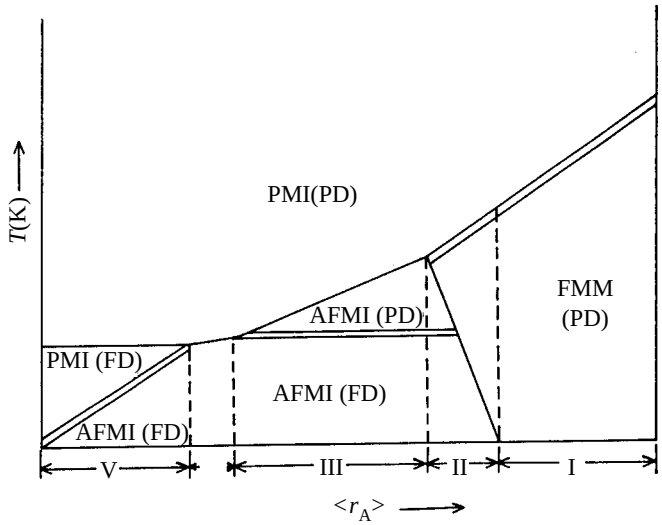

Figure 10. Schematic temperature–$\langle r_A \rangle$ phase diagram for $Ln_{0.5}A_{0.5}MnO_3$ showing different possible behaviours. Double line represents a second order transition and single line a first order transition. PD = paradistortive, FD = ferrodistortive (from Kumar & Rao 1997).

region V is distinctly different from that in region II, as is indeed observed experimentally.

Both the types of charge ordering discussed above are different from the charge density wave (CDW) type ordering caused by Fermi-surface nesting. These are more like the infinitely adaptive structures (Rao & Raveau 1995) and would occur over a continuous range of doping. Such lattice effects have been found in $La_{0.5}Ca_{0.5}MnO_3$ and $Nd_{0.25}La_{0.25}Ca_{0.5}MnO_3$. If one considers the blocking of the delocalization of e_g electrons by AFM or JT effects as an enhancement of the effective carrier mass, the CO state may indeed be viewed as Wigner crystallization at low temperatures, even for high carrier concentrations. In closing, it is pertinent to note that the spin, charge and orbital ordering exhibited by the rare-earth manganates is indeed unique and all these orderinga are closely intertwined with the metal–insulater transition in these materials.

References

Archibald, W., Zhou, J. S. & Goodenough, J. B. 1996 *Phys. Rev.* B **53**, 14 445.

Arulraj, A., Gundakaram, R., Rangavittal, N., Gayathri, N., Raychaudhuri, A. K. & Rao, C. N. R. 1998 *Phys. Rev.* B. (In the press.)

Asamitsu, A., Moritomo, Y., Kumai, R., Tomioka, Y. & Tokura, Y. 1996*a* *Phys. Rev.* B **54**, 1716.

Asamitsu, A., Moritomo, Y. & Tokura, Y. 1996*b* *Phys. Rev.* B **53**, 2952.

Biswas, A. & Raychaudhuri, A. K. 1996 *J. Phys. Condens. Matter.* **8**, L739

Brillinge, S. J. L., DiFrancesco, R. G., Kwei, G. H., Neumeier, J. J. & Thomson, J. D. 1996 *Phys. Rev. Lett.* **77**, 715.

Coey, J. M. D., Viret, M., Ranno, L. & Ounadjela, K. 1995 *Phys. Rev. Lett.* **75**, 3910.

De Teresa, J. M., Ibarra, M. R., Algarabel, P. A., Ritter, C., Garcia, J., del Moral, A. & Arnold, Z. 1997 *Nature* **386**, 250.

Edwards, P. P. & Rao, C. N. R. (eds) 1995 *Metal–insulator transitions revisited.* London: Taylor & Francis.

Edwards, P. P. & Sienko, M. J. 1978 *Phys. Rev.* B **17**, 2575.

Fontcuberta, J., Martinez, B., Seffar, A., Pinol, S., Garcia-Munoz, J. L. & Obradors, X. 1996 *Phys. Rev. Lett.* **76**, 1122.

Garcia-Munoz, J. L., Suaaidi, M., Fontcuberta, J. & Rodriguez-Carvajal, J. 1997 *Phys. Rev.* B **55**, 34.

Goodenough, J. P. 1971 *Progr. Solid State Chem.* **5**, 149.

Gundakaram, R., Arulraj, A., Vanitha, P. V., Rao, C. N. R., Gayathri, N., Raychaudhuri, A. K. & Cheetham, A. K. 1996 *J. Solid State Chem.* **127**, 354.

Hamilton, J. J., Keatley, E. L., Ju, H. L., Raychaudhuri, A. K. & Greene, R. L. 1996 *Phys. Rev.* B **54**, 14 926.

Hwang, H. Y., Cheong, S. W., Radaelli, P. G., Marezio, M. & Batlogg, B. 1995 *Phys. Rev. Lett.* **75**, 914 .

Ibarra, M. R., Algarabel, P. A., Marquina, C., Blasco, J. & Garcia, J. 1995 *Phys. Rev. Lett.* **75**, 3541.

Iye, Y. 1995 In *Metal–insulator transitions revisited* (ed. P. P. Edwards & C. N. R. Rao). London: Taylor & Francis.

Jonker, G. H. & van Santen, J. H. 1950 *Physica* **16**, 377.

Kimura, T., Tomioka, Y., Kuwahara, H., Asamitsu, A., Tamura, M. & Tokura, Y. 1996 *Science* **274**, 1698.

Kumar, N. & Rao, C. N. R. 1997 *J. Solid State Chem.* **129**, 363.

Kuwahara, H., Tomioka, Y., Asamitsu, A., Moritomo, Y. & Tokura, Y. 1995 *Science* **270**, 961.

Lynn, J. W., Erwin, R. W., Borchers, J. A., Huang, Q, Santoro, A., Peng, J. L. & Li, Z. Y. 1996 *Phys. Rev. Lett.* **76**, 4046.

Mahendiran, R., Mahesh, R., Rangavittal, N., Tewari, S. K., Raychaudhuri, A. K., Ramakrishnan, T. V. & Rao, C. N. R. 1996*a* *Phys. Rev.* B **53**, 3348.

Mahendiran, R., Mahesh, R., Raychaudhuri, A. K. & Rao, C. N. R. 1996*b* *Phys. Rev.* B **53**, 12 160.

Mahendiran, R., Mahesh, R., Raychaudhuri, A. K. & Rao, C. N. R. 1996*c* *Solid State Commun.* **99**, 149.

Mahendiran, R., Tiwari, S. K., Raychaudhuri, A. K., Mahesh, R. & Rao, C. N. R. 1996*d* *Phys. Rev.* B **54**, 9604.

Mahesh, R., Mahendiran, R., Raychaudhuri, A. K. & Rao, C. N. R. 1995 *J. Solid State Chem.* **120**, 204.

Mahesh, R., Mahendiran, R., Raychaudhuri, A. K. & Rao, C. N. R. 1996*a* *Appl. Phys. Lett.* **68**, 2291.

Mahesh, R., Mahendiran, R., Raychaudhuri, A. K. & Rao, C. N. R. 1996*b* *J. Solid State Chem.* **122**, 448.

Martin, M. C., Shirane, G., Endoh, Y., Hirota, K., Moritomo, Y. & Tokura, Y. 1996 *Phys. Rev.* B **53**, 14 285.

Millis, A. J., Littlewood, P. B. & Shraiman, B. I. 1996 *Phys. Rev.* B **53**, 8434.

Moritomo, Y., Asamitsu, A., Kuwahara, H. & Tokura, Y. 1996 *Nature* **380**, 141.

Mott, N. F. 1961 *Phil. Mag.* **6**, 287.

Mott, N. F. 1972 *Phil. Mag.* **26**, 1015.

Mott, N. F. 1982 *Proc. R. Soc. Lond.* A **382**, 1.

Okimoto, Y., Katsufuji, T., Ishikawa, T., Urushibara, A., Arima, T. & Tokura, Y. 1995 *Phys. Rev. Lett.* **75**, 109.

Park, J. H., Chen, C. T., Cheong, S. W., Bao, W., Meigs, G., Chakarian, V. & Idzerda, Y. 1996 *Phys. Rev. Lett.* **76**, 4215.

Radaelli, P. G., Marezio, M., Hwang, H. Y., Cheong, S. W. & Batlogg, B. 1996 *Phys. Rev.* B **54**, 8992.

Rao, C. N. R. 1989 *A. Rev. Phys. Chem.* **40**, 291.

Rao, C. N. R. 1996 *Chem. Commun.*, 2217.

Rao, C. N. R. & Ganguly, P. 1985 In *The metallic and the non-metallic states of matter* (ed. P. P. Edwards & C. N. R. Rao). London: Taylor & Francis.

Rao, C. N. R. & Ganguli, A. K. 1995 *Chem. Soc. Rev.* **24**, 1.

Rao, C. N. R. & Raveau, B. 1995 *Transition metal oxides*. New York: VCH.

Rao, C. N. R., Cheetham, A. K. & Mahesh, R. 1996 *Chem. Mater.* **8**, 2421.

Raychaudhuri, A. K. 1991 *Phys. Rev.* B **44**, 8572.

Roder, H., Zang, J. & Bishop, A. R. 1996 *Phys. Rev. Lett.* **76**, 1356.

Sarma, D. D., Shanti, N., Krishnakumar, S. R., Saitoh, T., Mizokawa, T., Sekiyama, A., Kobayashi, K., Fujimori, A., Weshchke, E., Meier, R., Kaindl, G., Takeda, Y. & Takano, M. 1996 *Phys. Rev.* B **53**, 6873.

Satpathy, S., Popovic, Z. S. & Vukajlovic, F. R. 1996 *Phys. Rev. Lett.* **76**, 960.

Snyder, J. G., Hiskes, R., Dicarolis, S., Beasley, M. R. & Geballe, T. H. 1996 *Phys. Rev.* B **53**, 14 434.

Thomas, G. A. 1983 *J. Phys. Chem.* **93**, 4414.

Tokura, Y., Tomioka, Y., Kuwahara, H., Asamitsu, A., Moritomo, Y. & Kasai, M. 1996 *J. Appl. Phys.* **79**, 5288.

Tyson, T. A., Mustre de Leon, J., Couradson, S. D., Bishop, A. R., Neumeier, J. J., Roder, H. & Zang, J. 1996 *Phys. Rev.* B **53**, 13 985.

Urushibara, A., Moritomo, Y., Arima, T., Asamitsu, A., Kido, G. & Tokura, Y. 1995 *Phys. Rev.* B **51**, 14 103.

Vogt, T., Cheetham, A. K., Mahendiran, R., Raychaudhuri, A. K., Mahesh, R. & Rao, C. N. R. 1996 *Phys. Rev.* B **54**, 15 303.

Yamada, Y., Hino, O., Noholo, S., Kanao, R., Inami, T. & Kotano, S. 1996 *Phys. Rev. Lett.* **77**, 904.

Zener, C. 1951 *Phys. Rev.* **82**, 403.

Zhao, G., Conder, K., Keller, H. & Muller, K. A. 1996 *Nature* **381**, 676.

Discussion

A. Möbius (*Institute for Solid State and Materials Research, Dresden, Germany*). To what extent do the critical temperatures for the metal–insulator and ferromagnetic–paramagnetic transitions coincide in $LaMnO_3$ and similar substances?

C. N. R. Rao. They are close to each other in many of the manganates, but they can differ significantly in samples of small particle size, prepared at relatively low temperatures.

A. Schofield (*Cavendish College, Cambridge, UK*). Professor Rao described how he could transform from 3d to 2d Mn perovskites by adding rock-salt layers. Has he ever seen behaviour similar to the high-T_c cuprates, where the behaviour is insulating in the c direction ($d\rho_c/dT < 0$) and metallic in the ab-plane ($d\rho_{ab}/dT > 0$)?

C. N. R. Rao. There is anisotropy in the layered manganates as well. Note that the single-layered manganate is an antiferromagnetic insulator while the two-layered manganate shows the insulator–metal transition.

D. M. Edwards (*Department of Mathematics, Imperial College, London, UK*). The ferromagnetic transition is clearly not a simple one. Perring's neutron data on CMR materials show beautiful spin waves over the whole zone at low temperatures. But these become strongly damped with increasing temperature long before T_c is reached. This must correspond to changes in electronic structure which are associated with the rapid rise in resistivity.

C. N. R. Rao. Across the T_c there is a structural change in the sense that Jahn–Teller distortion decreases in the ferromagnetic metallic phase.

A. S. Alexandrov (*Department of Physics, Lougborough University, UK*). Sir Nevill Mott wrote in his '65 years in physics' that his prediction of a minimum metallic conductivity $\sigma_{\min}$ was not completely correct. However, Professor Rao's experimental results show a $\sigma_{\min}$. Could he please comment on that?

C. N. R. Rao. I believe $\sigma_{\min}$ is a very useful quantity and signifies the value of conductivity across which the temperature coefficient of resistivity changes sign in many of the oxide materials. $\sigma_{\min}$ is a useful criterion at relatively high temperatures.

J. E. Enderby (*Department of Physics, University of Bristol, UK*). In order to make $n^{1/3}a_{\mathrm{H}}$ plots, it is necessary to know the dielectric constant and the electronic effective mass. Are these data available and/or reliable for all the systems in Professor Rao's diagram?

C. N. R. Rao. See Edwards & Sienko (1978) and also, more recently, Thomas (1983), who has estimated these for cuprates.

P. P. Edwards (*School of Chemistry, University of Birmingham, UK*). (i) I am heartened to hear that various 'simple' criteria (e.g. the Mott criterion, $\sigma_{\min}$, etc.) still represent highly effective operational prescriptors for metallization in these complex chemical compounds. I believe it will be important to add to this list the Herzfeld 'polarization catastrophe' model for complex oxides, possibly in the manner outlined by J. A. Duffy.

(ii) I completely agree with Professor Rao's view of the 'virtues of marginally metallic oxides' (Rao 1996) as *real chemical compounds* located close to the metal–non-metal transition.

C. N. R. Rao. I agree with these comments.

Additional references

Rao, C. N. R. 1996 *Chem. Commun.* 2217.

PHILOSOPHICAL TRANSACTIONS OF THE ROYAL SOCIETY A MATHEMATICAL, PHYSICAL & ENGINEERING SCIENCES